sustainability

MDPI

Article

Comparison of Different Power Generation Mixes for High Penetration of Renewables

Giovanni Brumana, Elisa Ghirardi * and Giuseppe Franchini

Department of Engineering and Applied Sciences, University of Bergamo, Marconi Street 5, 24044 Dalmine, Italy; giovanni.brumana@unibg.it (G.B.); giuseppe.franchini@unibg.it (G.F.)
* Correspondence: elisa.ghirardi@unibg.it; Tel.: +39-352052039

Abstract: Growing environmental concerns have driven the installation of renewable systems. Meanwhile, the continuous decline in the levelized cost of energy (LCOE), alongside the decreasing cost of photovoltaics (PVs), is compelling the power sector to accurately forecast the performance of energy plants to maximize plant profitability. This paper presents a comprehensive analysis and optimization of a hybrid power generation system for a remote community in the Middle East and North Africa (MENA) region, with a 10 MW peak power demand. The goal is to achieve 90 percent of annual load coverage from renewable energy. This study introduces a novel comparison between three different configurations: (i) concentrated solar power (parabolic troughs + thermal energy storage + steam Rankine cycle); (ii) fully electric (PVs + wind + batteries); and (iii) an energy mix that combines both solutions. The research demonstrates that the hybrid mix achieves the lowest levelized cost of energy (LCOE) at 0.1364 USD/kWh through the use of advanced transient simulation and load-following control strategies. The single-technology solutions were found to be oversized, resulting in higher costs and overproduction. This paper also explores a reduction in the economic scenario and provides insights into cost-effective renewable systems for isolated communities. The new minimum cost of 0.1153 USD/kWh underscores the importance of integrating CSP and PV technologies to meet the very stringent conditions of high renewable penetration and improved grid stability.

Keywords: power mix; renewable generation; energy storage

Citation: Brumana, G.; Ghirardi, E.; Franchini, G. Comparison of Different Power Generation Mixes for High Penetration of Renewables. *Sustainability* **2024**, *16*, 8435. https://doi.org/10.3390/su16198435

Academic Editor: Mosè Rossi

Received: 30 August 2024
Revised: 19 September 2024
Accepted: 23 September 2024
Published: 27 September 2024

1. Introduction

The growing need to address environmental concerns related to global warming is driving power generation systems toward a new paradigm by incorporating larger portions of renewable energy. An additional impetus is the declining levelized cost of electricity (LCOE), which is prompting many governments to design a new energy mix with the introduction of a significant amount of renewables [1]. Due to the high level of solar irradiation and favorable wind conditions, Middle Eastern and North African (MENA) countries are among the most suitable locations for renewable energy development, with many MENA governments actively transitioning their power generation systems to renewables, as reported by Poudineh et al. [2]. Some Gulf states have outlined visions to achieve up to 70 percent CO_2 reduction through the development of green plants [3]. Al Garni et al. [4] report an interesting renewable energy feasibility study based on capital projection in Saudi Arabia (up to 100 percent renewable generation). In Europe, although solar radiation is lower, there is promising wind potential. Frank et al. [5] discuss the optimal mix of wind and solar energy that ensures grid stability. Cole and Frazier [6] explore the impact of increasing renewable energy penetration on power systems, emphasizing that the uneven distribution of plants leads to poor system integration and requires enhanced grid flexibility and power generation modulation capacity. This new power generation mix can often cause load balance and grid stability problems because of the variability, intermittency, and unpredictability of renewable production. Several studies [7,8] highlight the need for energy storage integration into the electricity production system and its economic

impacts. Thermal energy storage (TES) is critical for power generation in concentrated solar power (CSP) plants, as it enables the storage of energy in high-density fluids, such as molten salts or diathermic oil, at medium to high temperatures with minimal losses. Li et al. [9] present a capacity planning model for a solar thermal power system with TES in electricity markets with high penetration of renewables, showing that while TES increases the LCOE, its use is justified by extended operation and environmental benefits. The real limitation of photovoltaics (PVs) and wind generation lies in electrochemical storage. The increasing production of Li-ion batteries and the associated economies of scale have resulted in substantial cost reductions, as reported by Verbruggen [10] and confirmed in the International Renewable Energy Agency (IRENA) report [11]. Achieving a high level of renewable penetration requires an optimized approach to system sizing to ensure a comprehensive techno-economic analysis and profitable design. Zurita et al. [12] explore this through a complex combination of CSP and PV hybrid plants, evaluating future cost reduction scenarios.

Optimization of the power generation mix has been a major focus in recent years, aiming to find the optimal solution to integrate renewable sources with energy storage. The paper by Seck et al. [13] addresses the optimization of renewable integration in the French power mix using a sophisticated grid simulation. The authors' conclusions underscore the importance of grid balance and interconnections. Similarly, Balaji and Gurgenci [14] assess the optimal power mix for an isolated Australian community with industrial (mining) and residential load profiles, taking into account both electricity costs and the environmental impacts of the optimization. The Red Sea Project [15], a resort development in the Kingdom of Saudi Arabia, has announced plans for 100 percent zero-carbon electricity generation, relying heavily on energy storage. For isolated communities or weakly interconnected grids, the challenge lies in defining the best power system configuration, which maximizes renewable energy contribution while matching demand profiles and maintaining grid stability. Energy management in these contexts is increasingly complex, and recent studies are addressing the issue of component sizing along with the best dispatch strategy. Ishraque et al. [16] compare different dispatch strategies for different locations in northern Bangladesh, concluding that the load-following strategy presents the lowest LCOE and emissions while ensuring a stable system response. Ramesh and Saini [17] emphasize the critical role of storage in grid management decisions, noting that operational constraints on batteries should be factored into load-following strategies to preserve battery life and minimize operating costs. More recent research, such as that presented by Vaziri Rad et al. [18], has shown the importance of demand-side management control, such as load shifting or deferrable load, in improving system performance over conventional dispatching strategies.

Building on previous studies of load-following strategies [19,20] and taking into account the guidelines set out in the review presented by Agajie et al. [21], the authors present in this paper an optimization procedure aimed at providing the lowest LCOE for a given fraction of renewable energy. The process determines the best generation mix, including PVs, wind turbines, CSP with TES, Li-ion batteries, and diesel generator sets (gensets). Based on the procedure presented in [22], the energy supply from each generation source and the size of the energy storage system (thermal and/or electrochemical) are determined with a complete techno-economic evaluation.

The main objectives of this research can be summarized as follows:

- Unlike models that deal with component details or management logic, the optimization procedure in this study is based on a numerical algorithm interacting with an accurate model of the entire multigeneration power system.
- A comparison of different renewable grids utilizing a load-following strategy is conducted, providing insights into the most effective technologies to increase the penetration of renewables in the stand-alone grid.
- To ensure a future-proof and cost-effective solution, this study also examines the potential evolution of the production mix under an economic scenario assuming technological advancements and cost reductions in the technologies considered.

2. Materials and Methods

The model is based on a load-following control strategy, where power demand is met by various power plants, including three renewable technologies: PVs, wind turbines, and CSP. Two types of energy storage are incorporated: thermal (molten salt tanks coupled with the CSP plant) and electrochemical (Li-ion batteries, available for any power surplus). The backbone of the multigeneration system is an AC bus, as depicted in Figure 1a. Electricity produced by the PV field and wind farm is transformed from DC to AC before entering the bus. The electric energy storage (EES) system is connected to the bus with an AC-to-DC rectifier and a DC-to-AC inverter. The efficiency of the inverter is set at 98% [23], while the efficiency of the rectifier is set at 82% [24]. The battery is assumed to be based on Li-ion technology, and the round-trip efficiency is equal to 90%, as reported by a manufacturer [25].

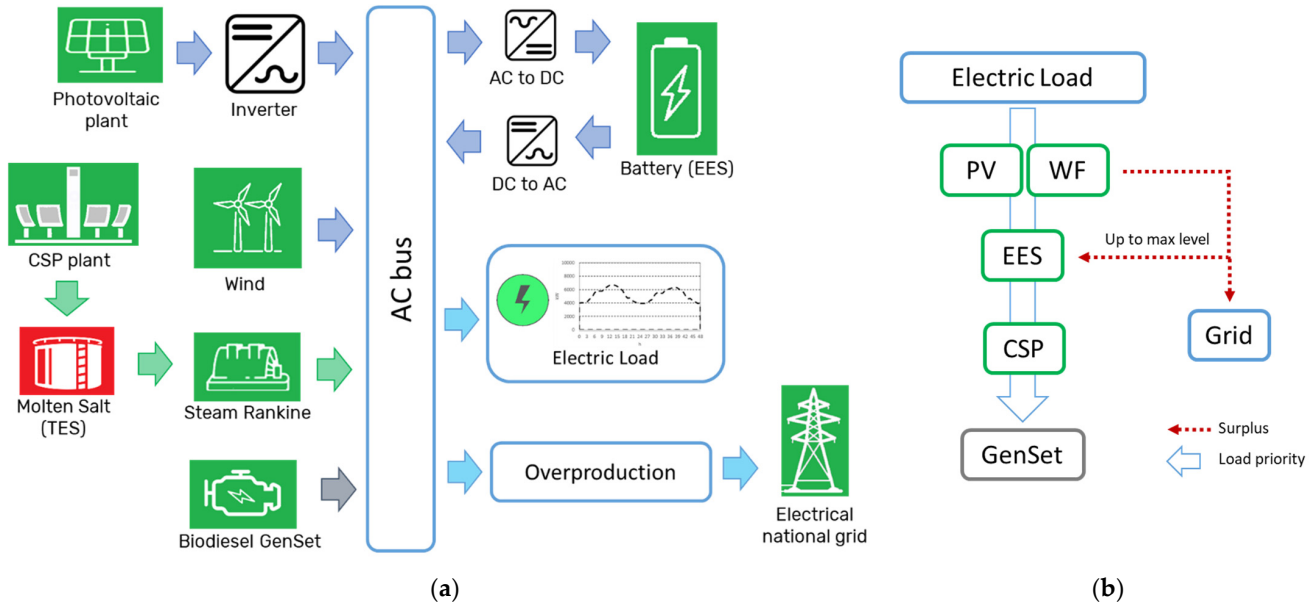

Figure 1. (**a**) Smart grid schematic, (**b**) control strategy schematic.

The control strategy adopted in the model aims to maximize the self-consumption of electricity. The CSP plant, utilizing parabolic trough collectors (PTCs), feeds a steam Rankine cycle with a double-tank molten salt thermal storage. Electricity from the PV field and wind farm is supplied directly to the AC bus, with any excess being stored in the battery system. A diesel genset is included in the model to cover residual load (10% annual load coverage) and ensure electricity supply in case of renewable power plant failures.

A control strategy has been implemented according to the following hierarchy, as shown in Figure 1b:

1. PV and wind farm electric production is supplied to the AC bus and to the load.
2. In the event of overproduction, the surplus is stored in the batteries (EES) according to their power limit (charge and discharge) and the state of charge.
3. If the batteries are fully charged, the overproduction from the wind farm and PV field is delivered to the grid.
4. In case the instantaneous outputs from the PVs and wind turbines are lower than the electrical load, the difference is provided by the batteries.
5. If the power demand still exceeds the available outputs of PVs + wind + EES, the deficit is covered by the CSP plant (PTC + TES).
6. If the electric load is greater than PV + wind + CSP production and the storage systems are depleted, the difference is covered by the auxiliary diesel genset.

2.1. Simulation Model

The model was developed using Trnsys 18 to simulate the entire multigeneration power system under a load-following operation. A transient simulation with a time step of 0.125 h was performed to accurately capture the dynamic behavior of the power plants over a one-year period under realistic operational conditions. The details of the models of each system are presented below.

2.1.1. Photovoltaic Field

The PV field model is based on manufacturer datasheets and includes the performance derating related to temperature variations and radiation levels. Table 1 outlines the key parameters of the selected PV modules. The PV field is modeled as a cluster of 100 kW_{dc} fields. The model also incorporates losses between the field and the AC bus (including 2% transportation, 18% power factor losses, and 2% inverter losses), as outlined in the design literature.

Table 1. PV module specifications.

Performance Characteristics	Unit	Value	Thermal Characteristics	Unit	Value
Maximum power (P_{max})	W	250	Nominal operating cell temp NOCT	°C	46
Open circuit voltage (V_{oc})	V	37.6	Temperature coefficient I_{sc}	%/°C	0.051
Maximum power point voltage (V_{mpp})	V	30.5	Temperature coefficient U_{oc}	%/°C	−0.31
Short circuit current (I_{sc})	A	8.81	Temperature coefficient P_{mpp}	%/°C	−0.41
Maximum power point current (I_{mpp})	A	8.27			
Efficiency (η_m)	%	14.91			

2.1.2. Wind Farm

The wind farm model is based on the performance curve of a reference wind turbine provided by the manufacturer. Each wind turbine has a nominal capacity of 2 MW. The main characteristics and operating parameters are listed in Table 2. Figure 2 shows the wind turbine's power curve as a function of wind speed, illustrating the electricity production of the wind farm time step by time step. In a wind farm, the power production does not include layout optimization and does not consider the interferences on downstream wind turbines.

Table 2. Wind turbine specifications.

	Unit	Value
Rotor diameter	m	76
Swept area	m^2	4500
Rotor speed max	rpm	16.0
Tipspeed	m/s	64
Power density	W/m^2	444.4

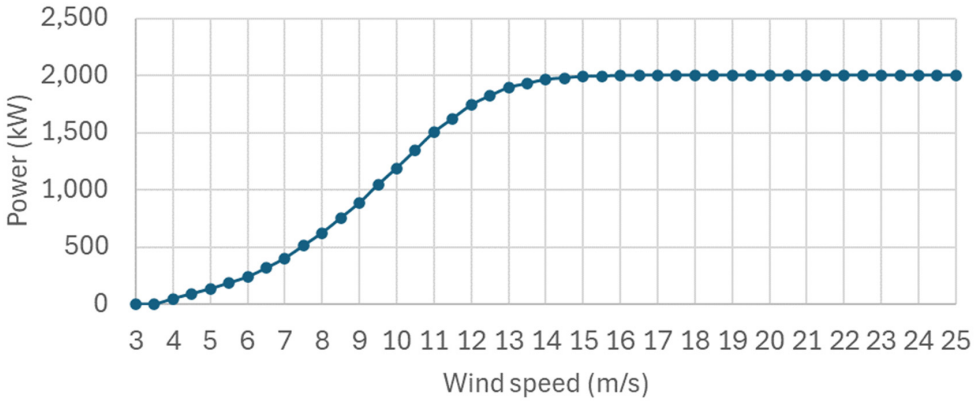

Figure 2. Wind turbine power curve.

2.1.3. CSP Plant

The CSP model is based on PTCs, with the solar field oriented along a north–south axis. The collectors are arranged in loops composed of a series of eight arrays, each with an aperture area of 524.8 m^2. The PTC efficiency is evaluated, time step by time step, according to Equation (1) presented in [26]. This equation considers the long-wave emission associated with the effective sky temperature (T_{sky}) and driven by the emissivity factor ε, as well as an estimate of the thermal losses due to the instantaneous wind speed (V_{wind}). Both terms are functions of the average fluid temperature inside the collector (T_{av}) and the direct normal irradiance (I_b). The equation also includes the coefficients η_{opt}, A, B, and C, which are related to the thermal efficiency curve of Schott PTR70 receivers under standard conditions [27]. The parameter K represents the incident angle modifier (IAM) as a function of the sunray incident angle.

$$\eta_{PTC} = \eta_{opt} \times K - (A + C \times V_{wind}) \times \frac{(T_{av} - T_{amb})}{I_b} - \varepsilon \times B \times \frac{\left({T_{av}}^4 - {T_{sky}}^4\right)}{I_b} \quad (1)$$

The model includes a two-tank thermal energy storage system that uses molten salt (60% $NaNO_3$–40% KNO_3) storage. The PTC design temperature is 550 °C, with the TES operating at 550 °C (hot tank) and 300 °C (cold tank). During sunny periods, molten salt heated by the solar field is stored in the hot tank and then delivered to the steam generator through a solar heat exchanger based on the mass flow rate required by the power block. After heat transfer, the molten salt is collected in the cold tank. The CSP model uses this storage to mitigate source fluctuations and store excess from the molten salt production.

A steam Rankine cycle driven by molten salt converts the heat collected by the solar field into electricity delivered to the grid. The model of the steam Rankine cycle accounts for the efficiency variation of the power block, considering factors such as design capacity, part-load conditions, and ambient temperature effects. The correlation between size and efficiency is derived from the results proposed by Poullikkas [28]. Considering that the expected power block capacity falls between 1 and 10 MW, an interpolation of the literature data represents an adequate solution. The interpolation function (Figure 3a), based on a polynomial function (solid line), fits the curve proposed by Poullikkas (dashed line) in the interval 500 kW_e–100 MW_e, with an R coefficient of 0.99. The operation map (Figure 3b) includes the part-load derating and ambient air temperature affecting the condenser performance. This map is normalized (100% load and 30 °C condenser temperature) to evaluate the power block performance at each time step. In particular, starting from the design capacity of the plant (proposed by the optimization tool), the software evaluates a performance map based on the steam turbine sizing. The design efficiency of the power block affects the real discharge time of the TES. In the simulation procedure, the developed algorithm evaluates the appropriate TES volume, ensuring it can satisfy the required storage operating time based on the power block's size and design efficiency.

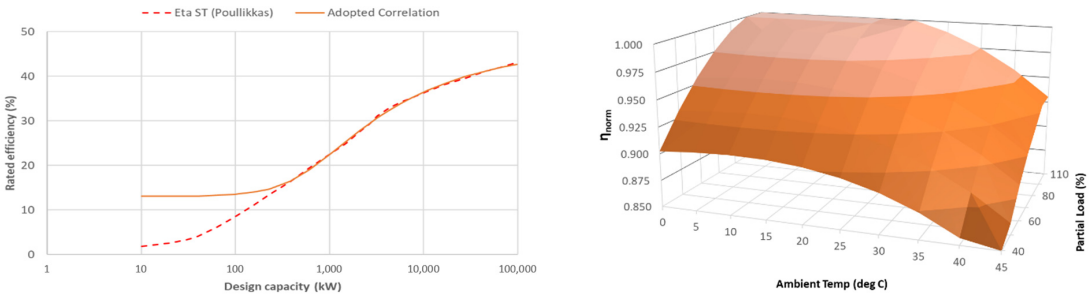

(**a**) (**b**)

Figure 3. Power block performance: (**a**) design efficiency vs. power block design output; (**b**) power block performance map normalized at 100% load and 30 °C.

2.2. Economic Evaluation

The model includes an updated analysis of component budget costs to improve the reliability of the economic evaluation.

PVs is currently one of the most cost-effective renewable technologies, with an LCOE as low as 0.067 USD/kWh. According to the "U.S. Solar Photovoltaic System Cost Benchmark," the global installed cost of a PV system is 1,100 USD/kW, with an operation and maintenance (O&M) cost of 9 USD/kW [29]. The IRENA report confirms this trend [30], citing module costs between 216 to 400 USD/kW, corresponding to total system costs ranging from 793 to 1210 USD/kW. Wind farms are also economically competitive, with an LCOE ranging from 0.046 USD/kWh for onshore turbines to 0.106 USD/kWh for offshore turbines. The cost for a land-based farm is about 1450–1600 USD/kW with an O&M cost of 20 USD/kW, as reported by the SAM software database (V2021.12.2) and the U.S. Energy Information Administration (EIA) outlook [31]. Notably, the IRENA report further suggests a possible reduction of up to 1000 USD/kW [30]. EES plays a key role in current and future PV-based energy plants, and its cost has steadily decreased in recent years. According to the cost benchmark in [29], the cost for a storage system based on a Li-ion battery is about 380 USD/kWh, corresponding to a 209 USD/kWh cost for a single battery component. Similarly, a battery cost of 176 USD/kWh is cited in the United Nations Environment Economic Division report [32].

In recent years, a minimum LCOE of 0.11 USD/kWh with fixed and variable O&M costs of 66 USD/kW and 0.004 USD/kWh, respectively, has been observed in CSP plants. Due to the complexity of CSP systems, a detailed cost evaluation is required for the main components considered in the optimization (aperture area, steam turbine capacity, and storage volume). The SAM software shows a PTC cost of 235 USD per unit aperture area, which is also confirmed by [33]. Analogously, a cost of 22 USD/kWh$_{th}$ is observed for the molten salt storage system. The typical cost for a 100 MW steam unit is about 1440 USD/kW [34]. Given the high dependence on power block size, the variable cost correlation proposed by Poullikkas et al. [28] has been adjusted in this work to align the results with this installed cost. The adopted power block cost function is shown in Figure 4, with the sum of all components representing the direct cost of the CSP plant. The total installed cost also includes indirect costs as a percentage of the direct costs (EPC—11%, contingency—7%, taxes—4%). For a 100 MW plant with 8 h TES, the total cost amounts to approximately 5500 USD/kW, which is comparable to the 3400–5200 USD/kW range proposed in the report [30].

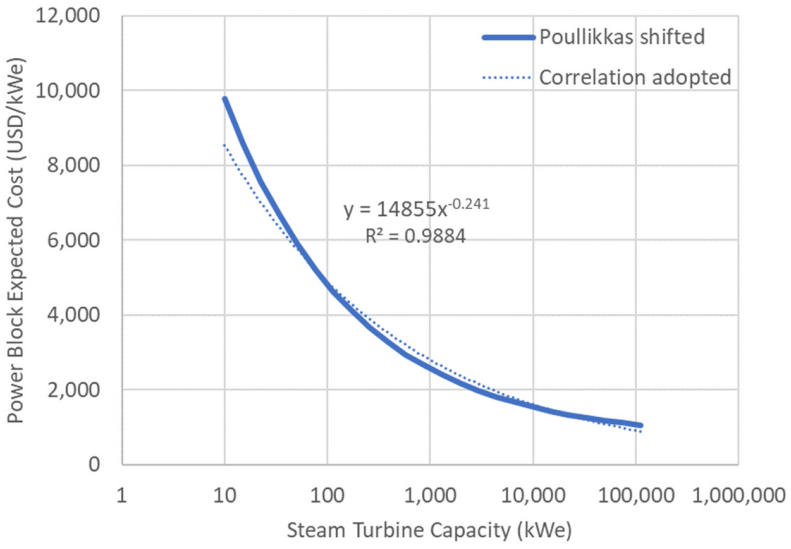

Figure 4. Power block expected cost (modified from [28]).

According to the cost data reported in the literature, the unit costs of the components used in this study are listed in Table 3, while the O&M costs are detailed in Table 4, distinguishing between fixed and variable costs. In addition, a new scenario (Scenario 2) has been introduced based on the reduction trend reported in the literature [30]. A minimum cost of 793 USD/kW is reported for PVs, and a reduction to 1000 USD/kW is expected for onshore wind turbines. Given a reported constant reduction in battery price of 15% per year, a battery cost close to 325 USD/kW can be expected [32]. By contrast, CSP plants are shown to reduce costs to a limited extent, and PTC costs are projected to be 6% lower than the actual. TES and steam power block costs are assumed to remain constant over the years.

Table 3. Installation costs.

Power Plant		Standard Cost (Scenario 1)	Expected Trend Cost (Scenario 2)
Photovoltaics	USD/kW	1210	793
Parabolic Trough Collectors	USD/m^2	235	220
Wind turbine	USD/kW	1497	1000
Steam power block	USD/kW	Size-dependent	Size-dependent
Storage			
Molten Salt	USD/kWh$_{th}$	22	22
Battery storage (Li-ion)	USD/kWh$_e$	380	325

Table 4. Operation and maintenance costs.

Technology	Fixed	Variable
PV	9 USD/kW	
CSP	66 USD/kW	4 USD/MWh
Wind turbine	44 USD/kW	
Battery storage	10 USD/kW	3.1 USD/MWh

The LCOE is used as a metric for comparing different power mix combinations. For each plant, the analysis takes into account its individual lifetime and the annual degradation as a fraction of the first year's energy production, as shown in Table 5. It is worth noting that the battery storage lifetime of 10 years is related to a large depth of discharge. By the end of its life, the battery's capacity is projected to decrease by 20%. Moreover, the PTC degradation encompasses optical degradation, vacuum losses, and mirror aging.

Table 5. Lifespan and annual degradation.

Component	Lifetime (LT)	Annual Degradation	
Photovoltaics	20	1%	
Wind turbine	25	0.7%	[35]
CSP—PTC	30	0.5%	[33,36]
Battery storage	10	3%	[37,38]

The LCOE for the power mix has been calculated as a weighted average of the individual technology LCOEs, as shown in Equation (2). This method represents a novel approach compared to the standard formula. Here, the LCOE of each component is considered separately, with a specific lifetime and aging degradation. This means that, at the end of the PVs lifetime, for example, the PV system will be replaced with a new one without affecting the other components. Equation (3) calculates the total power over the lifetime ($prod_{PV}$), taking the PV system as an example. Specifically, the terms are as follows:

- The lifetime global derating ($prodLT_{PV}$) as the average of the annual derating (der_{PV}), as stated in Equation (4);
- The annual energy production ($prod_{y,PV}$) computed according to the load-following control strategy in the system's first year of operation;

- The lifetime of the technology (LT_{PV}).

The single-technology *LCOE* was computed according to the classical formula (Equation (5)), which includes the global plant cost ($C_{plant,PV}$), the annual energy production ($prod_{y,i}$), and the O&M costs previously presented in Table 4. For each technology, the *CF* factor (Equation (6)) is also taken into account based on the lifetime (LT_{PV}) and the interest rate (i); it is assumed to be 4% of the installation cost.

$$LCOE\ (\text{USD/kWh}_\text{e}) = \frac{LCOE_{PV} \times prod_{PV} + LCOE_{batt} \times prod_{batt} + LCOE_{WF} \times prod_{WF} + LCOE_{CSP} \times prod_{CSP}}{prod_{PV} + prod_{batt} + prod_{WF} + prod_{PTC}} \quad (2)$$

$$prod_{PV}(\text{kWh}_\text{e}) = prodLT_{PV} \times prod_{y,PV} \times LT_{PV} \quad (3)$$

$$prodLT_{PV} = \frac{1}{LT_{PV}} \sum_{1}^{LT} der_{PV} \quad (4)$$

$$LCOE_{PV}\ (\text{USD/kWh}_\text{e}) = \frac{CF_{PV} \times C_{plant,PV}}{prod_{y,PV}} + OM \quad (5)$$

$$CF_{PV} = \frac{i(1+i)^{LT_{PV}}}{(1+i)^{LT_{PV}} - 1} \quad (6)$$

2.3. Optimization Procedure

The model of the power mix was optimized using the software GenOpt (Version 2.1.0), a tool developed by Berkley University [39]. GenOpt executes multiple annual Trnsys simulations to select the best configuration that minimizes the objective function defined in Equation (7). A double-step optimization process combining the particle swarm algorithm and the Hooke and Jeeves algorithm was employed to improve the identification of global optimum solutions. The optimization procedure was based on the global LCOE (Equation (2)) minimization under the limit of a renewable fraction (RF) equal to 90 percent. The residual part of the load (10%) was assumed to be covered by a biofuel genset. A penalty factor was included in the LCOE evaluation to force the optimization tool to reject the solutions under the selected RF. Considering the degradation of the equipment, it was assumed that the RF is guaranteed in the first year of operation.

$$f_{min} = LCOE + Penalty_{(RF<RF90\%)} \quad (7)$$

The optimization was performed to achieve the best configuration under three different plant configurations, as presented in Table 6:

i. Optimal CSP configuration (PTC + steam turbine + molten salt TES);
ii. Optimal electric combination (PVs + wind + EES);
iii. Optimal power mix configuration.

Table 6. Plant configurations.

Configuration	(i)—CSP	(ii)—PV + WF	(iii)—MIX
Technology	CSP	PV + WF	PV + WF + CSP
Storage	Molten salt TES	EES	EES + Molten salt TES
Renewable fraction target	90%	90%	90%

The optimization variables and their search space are reported in Table 7.

Table 7. Optimization variables (starting value—minimum value—maximum value—step) and parameters.

		i—CSP	ii—PV + WF	iii—MIX
PVs	MW_e	–	12–6–60–2	10–4–20–1
Wind turbine	MW_e	–	12–0–24–1	4–0–12–1
Battery capacity	MWh_e	–	40–12–80–2	3–0–10–0.5
PTC aperture area	m^2/MW_e	18,900–2100–42,000–1050	–	18,900–2100–42,000–1050
TES storage	h	12–2–24–0.5	–	12–2–24–0.5
Steam turbine output	MW_e	10–0.5–15–0.5	–	10–2–15–0.5

2.4. Meteorological Data and Electric Load

For this study, the system was assumed to be located in Tabuk (Kingdom of Saudi Arabia), a region with favorable direct normal irradiance (DNI) and wind conditions throughout most of the year. The area's low humidity levels—both in summer and winter—help minimize the diffusion of solar radiation, enhancing the efficiency of solar concentrators [40]. Table 8 provides an overview of the annual solar radiation, while Figure 5 shows the wind intensity and its duration curve. The potential of the site is well represented by the 5452 h of wind speeds exceeding 3 m/s. Meteorological data used in the Trnsys model are from the Meteonorm database.

Table 8. Site meteorological data.

Latitude–Longitude	28°23′ N 36°35′ E
DNI (kWh/m^2y)	2098
GHI (kWh/m^2y)	2069
Wind (>3 m/s) (h/y)	5452

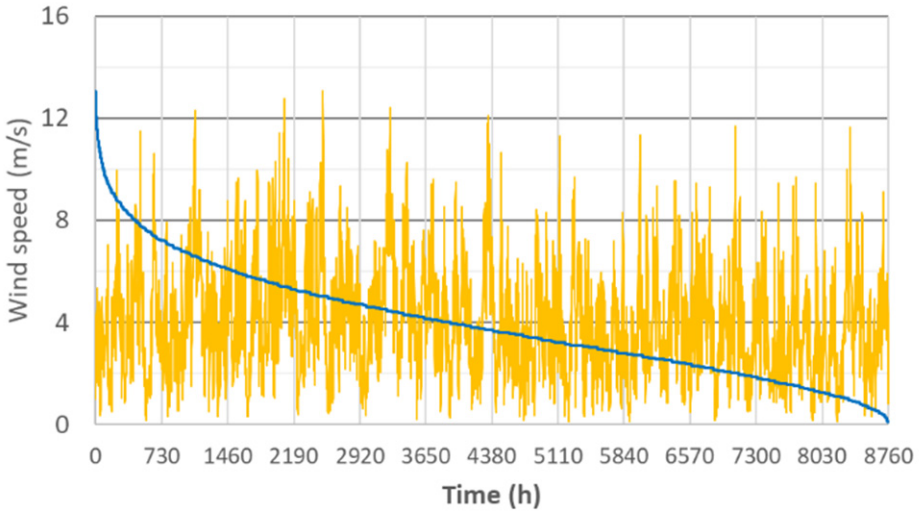

Figure 5. Site annual solar irradiance and wind speed (Meteonorm database).

The model was designed to evaluate the multigeneration power plant performance under a load-following control strategy. The electric load data were derived from the Abu Dhabi Annual Technical Report, as adopted in a previous study [41]. The annual demand (Figure 6) was scaled down to reach 10 MW peak load and an annual amount of 53.93 GWh.

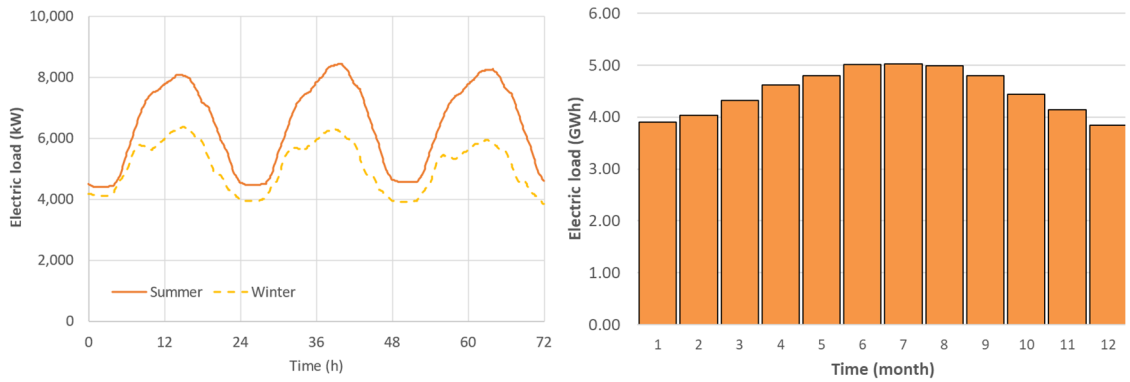

(**a**) (**b**)

Figure 6. Electric load: (**a**) hourly values in a 3-day period (summer and winter); (**b**) monthly values.

3. Results

3.1. Sizing Optimization

The results of the sizing optimization for each plant configuration are presented below. The optimization procedure identifies the optimal combinations of variables (as detailed in Table 7) that achieve 90 percent coverage of the annual load by renewable sources. Figure 7 shows the optimal size of each component based on the Scenario 1 budget costs: red represents the CSP configuration (i), blue represents PV + WF (ii), and green represents the power mix (iii). The optimum for case (i) exhibits a power block capacity of 10 MW and a TES of 115 MWh. The solar field has a total aperture area of 300,000 m^2. The design power output is much higher in case (ii) (40 MW PV + 18 MW WF), while the electrochemical energy storage capacity is very low (66 MWh). These results confirm the dispatchability of CSP technology compared to PV and wind power. Moving to case (iii), the optimal mix shows a cumulative capacity of 28.5 MW. The PV size is half of the configuration (ii), while the WF capacity is reduced to almost zero. The algorithm converges on a configuration in which nighttime power is supplied by the TES storage, which remains large (111 MWh). On the contrary, the contribution of the EES is negligible.

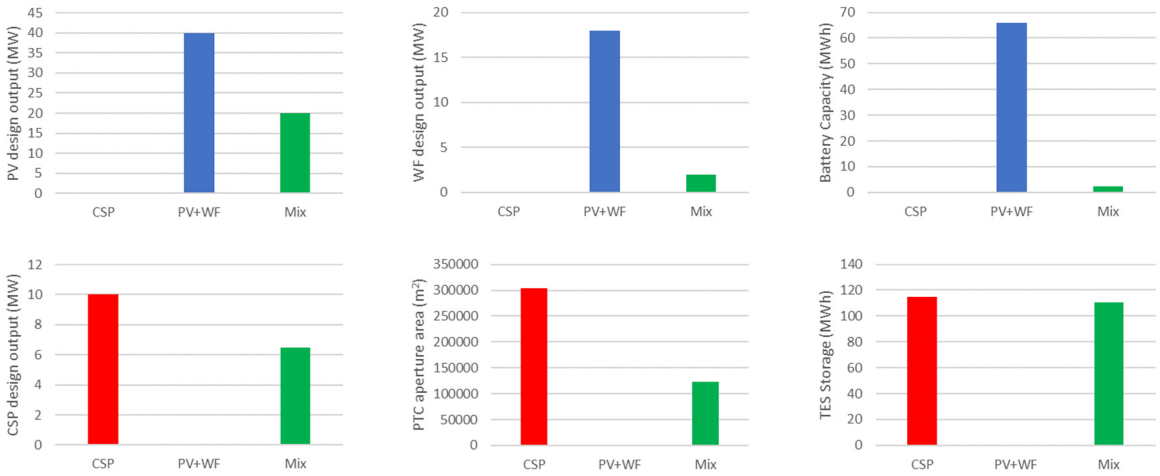

Figure 7. Optimal sizing for "Scenario 1".

Despite the significant variation in the expected budget costs, the optimization results for Scenario 2 are remarkably similar, as shown in Table 9. The component sizing is almost unchanged, with only a slight reduction in the CSP plant in favor of the WF in case (iii). In fact, the 35% cost reduction of wind turbines makes the WF a preferable solution for nighttime production.

Table 9. Optimization results and comparison of the two economic scenarios (1–2).

		i—CSP	ii—PV + WF	iii—MIX
PVs	MW_e	-	40–40	20–18
Wind turbine	MW_e	-	18–22	2–9
Battery capacity	MWh_e	-	66–62	2.25–1.75
PTC aperture area	m^2/MW_e	305,000–303,000	-	123,000–91,000
TES storage	MWh	115–118	-	111–90
Steam turbine output	MW_e	10–10	-	6.50–5.75

3.2. Hourly Simulation Results

To appreciate the advantages of the mixed configuration, it is essential to analyze the hourly simulation results. Figure 8 illustrates the three-day periods in both summer and winter across the three investigated configurations.

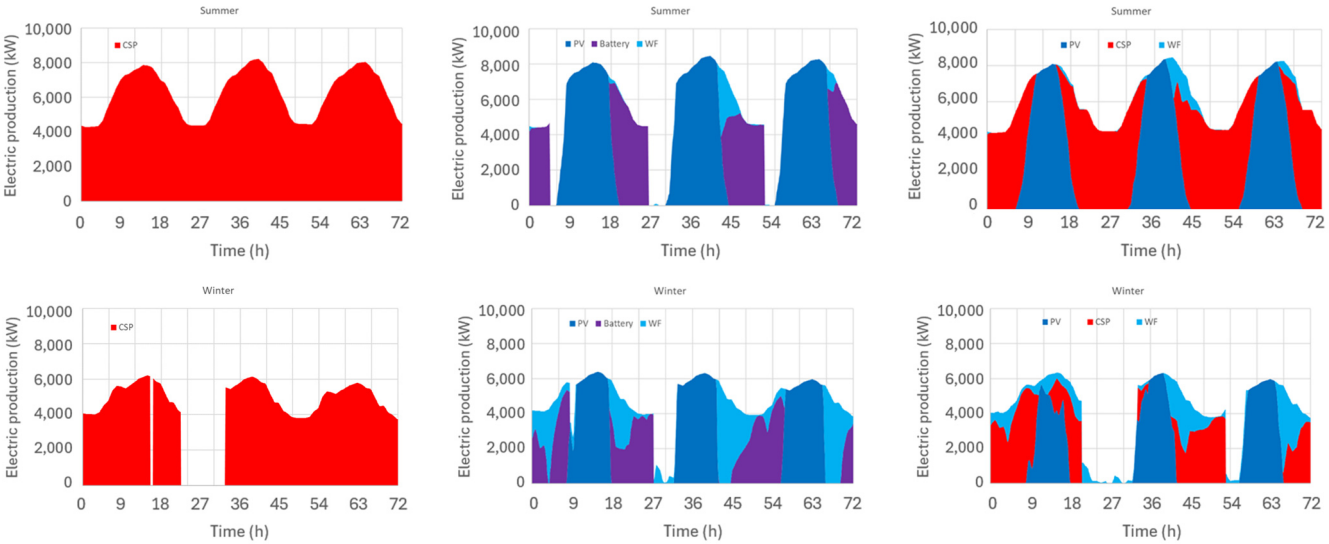

Figure 8. Hourly simulation results (3-day period): (**a**) i—CSP, (**b**) ii—PV + WF, (**c**) iii—Mix.

Figure 8a is related to the CSP plant. The large aperture area ensures full load coverage in summer, but various plant shutdowns take place in winter. To achieve the given RF, the plant must be oversized. Therefore, in summer, several troughs must be defocused for many hours per day since the hot storage tank is at maximum capacity. Meanwhile, Figure 8b shows the power production of the PV + WF system. This configuration performs similarly in summer and winter. It is evident that wind power is directly delivered to the grid at night, whilst PV power is prioritized during sunny hours. The complementarity of the three power generation systems (CSP, PVs, and WF) is elucidated in Figure 8c. In summer, the TES of the CSP plant enables full load coverage by storing solar energy during the day and making it available at night. In winter, part of the night load is supplemented by the backup genset.

Figure 9a shows the annual electricity production of the three configurations. The gray segment represents the overproduction. For the CSP plant (where trough defocus is assimilated to overproduction) and the PV + WF configuration, overproduction amounts to around 40% of the total production. However, the overproduction of the power mix drops to 23% as the production is efficiently distributed between CSP and PV power.

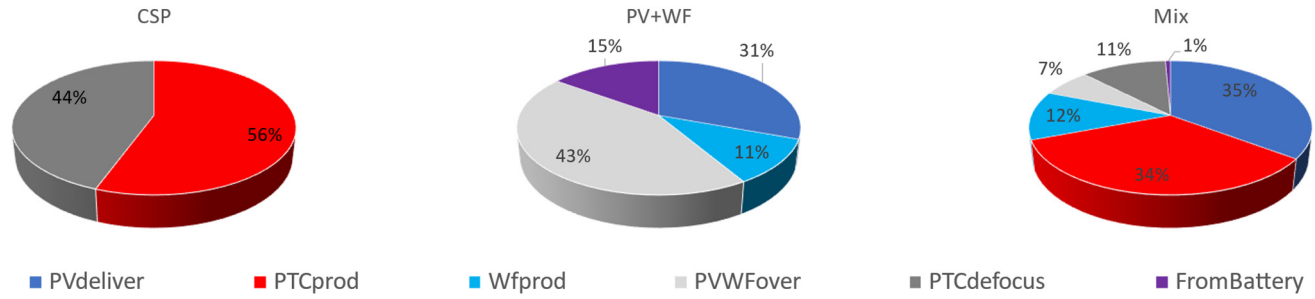

(**a**)

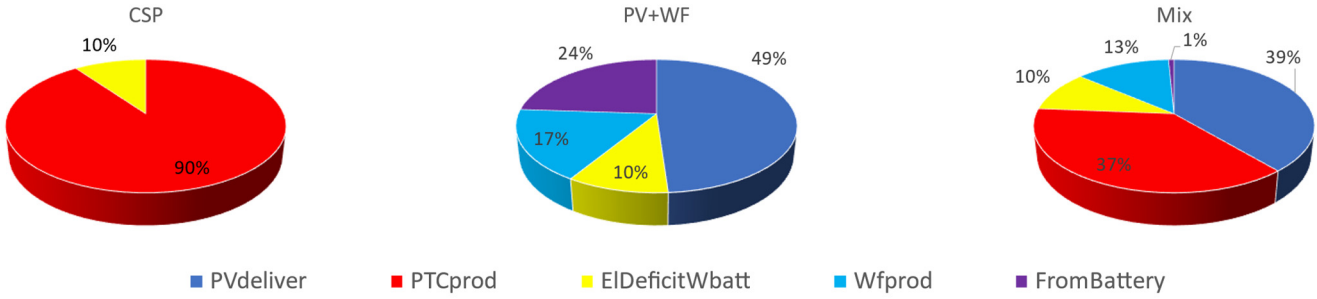

(**b**)

Figure 9. Annual performance: (**a**) electricity production, (**b**) electric load contribution of each technology.

Figure 9b shows the technology-specific contribution to the electric load. The yellow segments refer to the energy produced by the genset (10%). It is worth noting that in case (iii), the supplied PV energy reaches close to 50%, similar to case (ii), despite the PV capacity being halved in the mixed configuration.

Figure 10 compares the monthly energy production of the three configurations with the electrical load. The bar chart confirms that power production is more stable throughout the year for the PV + WF configuration, while the CSP plant exhibits more pronounced seasonal variations.

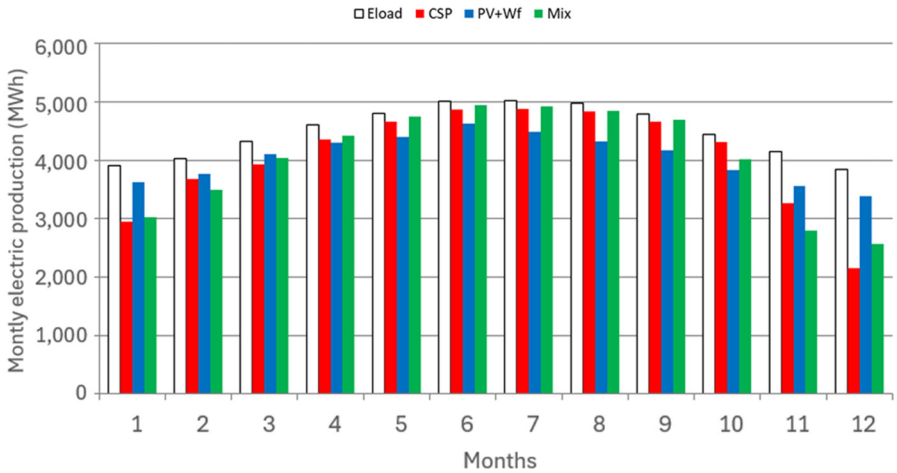

Figure 10. Monthly energy production and electric load.

Figure 11 shows the monthly energy production share for each configuration. The yellow segments (deficit) indicate the diesel genset contribution. The CSP plant (Figure 11a) exhibits more pronounced seasonal variations compared to the PVs + WF case (Figure 11b), where the electricity delivered to the grid via batteries is around 20% of the monthly load

for the whole year. In the power mix case (Figure 11c), CSP production predominates between May and October, while PV generation leads from November to April.

(**a**) (**b**) (**c**)

Figure 11. Share of monthly energy production: (**a**) i—CSP, (**b**) ii—PV + WF, (**c**) iii—Mix.

3.3. Economic Results

The optimization results are presented and discussed from an economic perspective. Figure 12 shows the minimum LCOE for all cases and both scenarios. The results are strongly affected by the constraint of a very high renewable fraction. The CSP option shows a lower LCOE compared to case (ii) (PV + WF) despite the higher installation cost per unit of power. This is due to the aforementioned oversizing of the PV section and the high cost of EES. The hybrid system (iii) allows the attainment of the best performance with an LCOE of 0.1364 USD/kWh. The economic results for Scenario 2 exhibit a similar trend, with a major reduction for case (ii), according to the estimated cost variations.

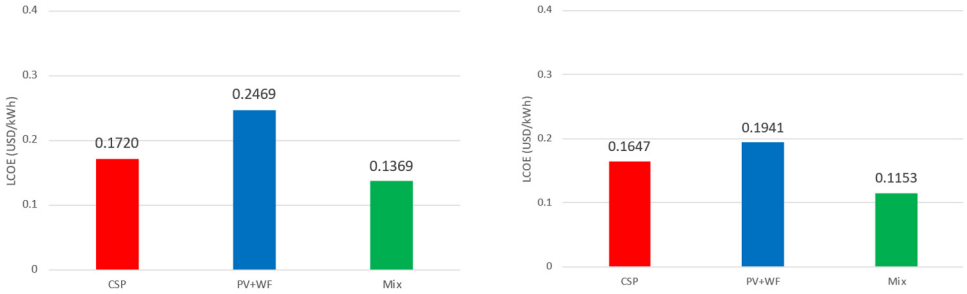

(**a**) (**b**)

Figure 12. Minimum LCOE: (**a**) Scenario 1; (**b**) Scenario 2.

Figure 13a,b show the LCOE composition for Scenarios 1 and 2, respectively. The CSP configuration is not presented in this analysis, as the cost is attributed to a single component. The result of the PV + WF layout shows that the electric energy storage, with an LCOE close to 0.40 USD/kWh, is the component responsible for the high cost of the electricity produced (0.2469 USD/kWh). Nevertheless, in the case of the mixed layout, the unitary cost of the electricity provided by the battery is still high, but due to the low-capacity installation, the global LCOE is not affected. The LCOE of the wind farm is higher in the PV–WF system due to the unpredictability of the resource. To guarantee the selected RF, the system requires an oversized plant with a high level of overproduction. The cost of PTC-based electricity is higher with respect to PVs, but the mix allows the adoption of a low-cost TES with the advantages of sunny-hour production of PV plants. Moreover, PV and wind farms are components that reduce the overall cost of electricity, while the CSP and battery essentially facilitate night operations and the desired renewable fraction. The adoption of the Scenario 2 cost improves the LCOE value, but the constraints of the optimization force the algorithm to keep the CSP plant. The results show that, regardless of individual component costs, achieving high renewable penetration benefits from combining different technologies.

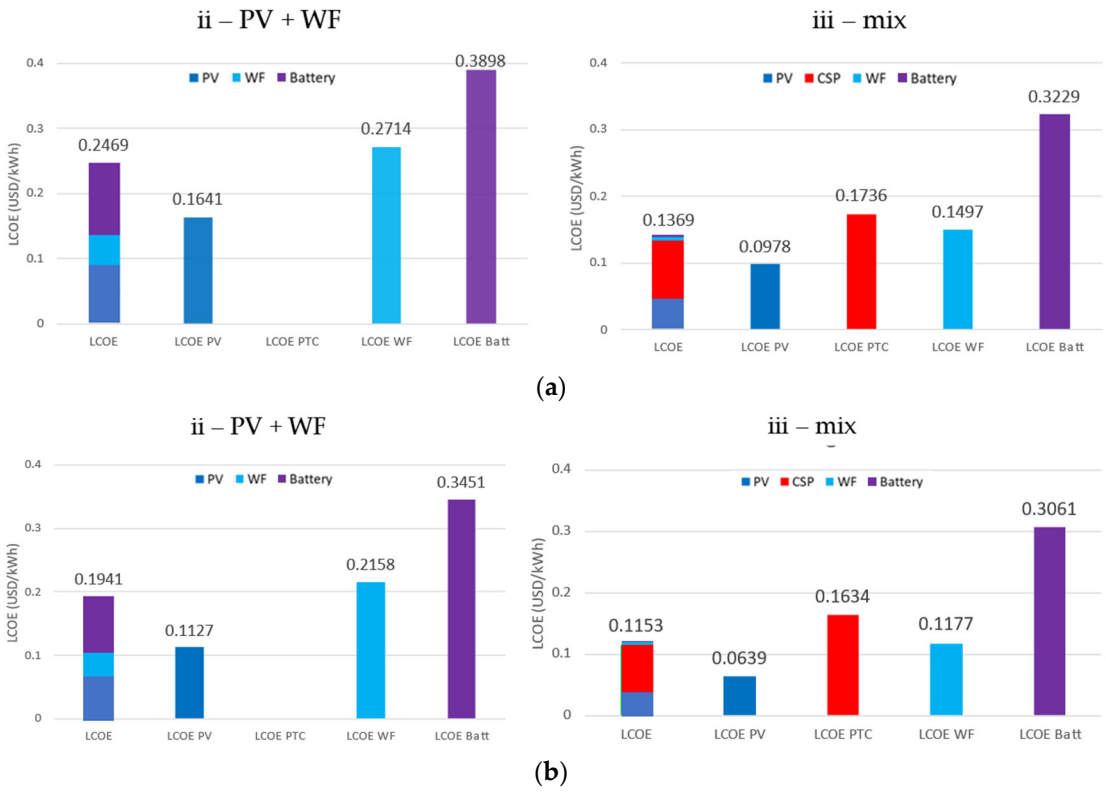

Figure 13. LCOE breakdown for each configuration: (**a**) Scenario 1; (**b**) Scenario 2.

4. Conclusions

In this work, a comprehensive model of a power mix has been evaluated, including an optimization procedure to ensure the lowest LCOE for a high renewable energy share (90%). This procedure is based on an accurate modeling of each component within the whole multigeneration power system and is applied to a case study in a remote community in Saudi Arabia. The power mix is optimized using a load-following operation simulation and compared to full electric solutions involving PV and wind farms, as well as a CSP solution. The adoption of the optimized power mix shows a consistent reduction in component sizing. The required PV capacity is half that of a full PV–WF configuration. Similarly, the CSP plant reduces the power block capacity and PTC aperture area compared to a full CSP solution. Meanwhile, the TES storage is kept very large to evaluate the night load.

From an economic vantage point, the optimization shows a significant reduction in the LCOE when transitioning from a single-technology solution to an optimized hybrid system. The CSP solution offers a better result compared with the all-electric solution due to the high unit cost of EES. The LCOE reported by the CSP plant is 26% higher with respect to the mix but 30% lower with respect to the fully electric system. The adoption of a reduced cost scenario influences the PV–WF solution with a consistent LCOE reduction (−27%) with respect to the actual budget costs. Otherwise, the hybrid configuration benefits less (−18%) from this cost reduction due to the lower variation of the unit cost of the CSP components.

Author Contributions: Conceptualization, G.B., E.G. and G.F.; methodology, G.B.; software, G.B. and E.G.; validation, E.G. and G.F.; data curation, E.G.; writing—original draft preparation, G.B.; writing—review and editing, G.B. and E.G.; supervision, G.F. All authors have read and agreed to the published version of the manuscript.

Funding: This research received no external funding.

Institutional Review Board Statement: Not applicable.

Informed Consent Statement: Not applicable.

Data Availability Statement: Data inquiries can be directed to the corresponding author.

Conflicts of Interest: The authors declare no conflicts of interest.

References

1. Said, Z.; A Alshehhi, A.; Mehmood, A. Predictions of UAE's renewable energy mix in 2030. *Renew. Energy* **2018**, *118*, 779–789. [CrossRef]
2. Poudineh, R.; Sen, A.; Fattouh, B. Advancing renewable energy in resource-rich economies of the MENA. *Renew. Energy* **2018**, *123*, 135–149. [CrossRef]
3. Alatiq, A.; Aljedani, W.; Abussaud, A.; Algarni, O.; Pilorgé, H.; Wilcox, J. Assessment of the carbon abatement and removal opportunities of the Arabian Gulf Countries. *Clean Energy* **2021**, *5*, 340–353. [CrossRef]
4. Al Garni, H.Z.; Mas'ud, A.A.; Wright, D. Design and economic assessment of alternative renewable energy systems using capital cost projections: A case study for Saudi Arabia. *Sustain. Energy Technol. Assess.* **2021**, *48*, 101675. [CrossRef]
5. Frank, C.; Fiedler, S.; Crewell, S. Balancing potential of natural variability and extremes in photovoltaic and wind energy production for European countries. *Renew. Energy* **2020**, *163*, 674–684. [CrossRef]
6. Cole, W.; Frazier, A.W. Impacts of increasing penetration of renewable energy on the operation of the power sector. *Electr. J.* **2018**, *31*, 24–31. [CrossRef]
7. de Sisternes, F.J.; Jenkins, J.D.; Botterud, A. The value of energy storage in decarbonizing the electricity sector. *Appl. Energy* **2016**, *175*, 368–379. [CrossRef]
8. Leonard, M.D.; Michaelides, E.E.; Michaelides, D.N. Energy storage needs for the substitution of fossil fuel power plants with renewables. *Renew. Energy* **2019**, *145*, 951–962. [CrossRef]
9. Li, J.; Lu, T.; Yi, X.; An, M.; Hao, R. Energy systems capacity planning under high renewable penetration considering concentrating solar power. *Sustain. Energy Technol. Assess.* **2024**, *64*, 103671. [CrossRef]
10. Energy Storage Picks Up Pace as Costs Fall. Available online: https://www.windpowermonthly.com/article/1523664?utm_source=website&utm_medium=social (accessed on 18 September 2024).
11. Ralon, P.; Taylor, M.; Ilas, A.; Diaz-Bone, H.; Kairies, K.-P. *Electricity Storage and Renewables: Costs and Markets to 2030*; International Renewable Energy Agency: Abu Dhabi, United Arab Emirates, 2017.
12. Zurita, A.; Mata-Torres, C.; Valenzuela, C.; Felbol, C.; Cardemil, J.M.; Guzmán, A.M.; Escobar, R.A. Techno-economic evaluation of a hybrid CSP + PV plant integrated with thermal energy storage and a large-scale battery energy storage system for base generation. *Sol. Energy* **2018**, *173*, 1262–1277. [CrossRef]
13. Seck, G.S.; Krakowski, V.; Assoumou, E.; Maïzi, N.; Mazauric, V. Embedding power system's reliability within a long-term Energy System Optimization Model: Linking high renewable energy integration and future grid stability for France by 2050. *Appl. Energy* **2019**, *257*, 114037. [CrossRef]
14. Balaji, V.; Gurgenci, H. Search for optimum renewable mix for Australian off-grid power generation. *Energy* **2019**, *175*, 1234–1245. [CrossRef]
15. The Red Sea. Available online: https://www.redseaglobal.com/en/our-destinations/the-red-sea (accessed on 18 September 2024).
16. Ishraque, F.; Shezan, S.A.; Ali, M.; Rashid, M. Optimization of load dispatch strategies for an islanded microgrid connected with renewable energy sources. *Appl. Energy* **2021**, *292*, 116879. [CrossRef]
17. Ramesh, M.; Saini, R.P. Dispatch strategies based performance analysis of a hybrid renewable energy system for a remote rural area in India. *J. Clean. Prod.* **2020**, *259*, 120697. [CrossRef]
18. Rad, M.A.V.; Kasaeian, A.; Mahian, O. Evaluation of stand-alone hybrid renewable energy system with excess electricity minimizer predictive dispatch strategy. *Energy Convers. Manag.* **2024**, *299*, 117898.
19. Brumana, G.; Franchini, G.; Ghirardi, E. Investigation of the Load-Following Capability of CSP Plants. *Energy Procedia* **2018**, *148*, 615–622. [CrossRef]
20. Ghirardi, E.; Brumana, G.; Franchini, G.; Perdichizzi, A. The optimal share of PV and CSP for highly renewable power systems in the GCC region. *Renew. Energy* **2021**, *179*, 1990–2003. [CrossRef]
21. Agajie, T.F.; Ali, A.; Fopah-Lele, A.; Amoussou, I.; Khan, B.; Velasco, C.L.R.; Tanyi, E. A Comprehensive Review on Techno-Economic Analysis and Optimal Sizing of Hybrid Renewable Energy Sources with Energy Storage Systems. *Energies* **2023**, *16*, 642. [CrossRef]
22. Brumana, G.; Franchini, G.; Ghirardi, E.; Perdichizzi, A. Techno-economic optimization of hybrid power generation systems: A renewables community case study. *Energy* **2022**, *246*, 123427. [CrossRef]
23. String Inverters—PVS300, 3.3 to 8.0 kW. Available online: http://www.renewpowers.com/datasheets/ABB/ABB%20String%20Inverters.pdf (accessed on 18 September 2024).
24. High Efficiency Wideband Three-Phase Rectifiers and Adaptive Rectifier Management for Telecom Central Office and Large Data Center Applications. Available online: https://www1.eere.energy.gov/manufacturing/datacenters/pdfs/adaptive_rectifier_ppt.pdf (accessed on 18 September 2024).
25. Tesla PowerPack Datasheet. Available online: https://impulsoragdl.com/wp-content/uploads/2020/09/Ficha-Tecnica-Power-Pack.pdf (accessed on 18 September 2024).

26. Simulation of the Part-Load Behaviour of a 30 MW SEGS Plant. Available online: https://www.osti.gov/servlets/purl/95571/ (accessed on 18 September 2024).
27. Final Test Results for the Schott HCE on a LS-2 Collector. Available online: https://digital.library.unt.edu/ark:/67531/metadc931115/ (accessed on 18 September 2024).
28. Poullikkas, A.; Rouvas, C.; Hadjipaschalis, I.; Kourtis, G. Optimum Sizing of Steam Turbines for Concentrated Solar Power Plants. *Int. J. Energy Environ.* **2012**, *3*, 9–18.
29. U.S. Solar Photovoltaic System Cost Benchmark: Q1 2018. Available online: https://www.nrel.gov/docs/fy19osti/72399.pdf (accessed on 18 September 2024).
30. Anuta, H.; Ralon, P.; Taylor, M. Renewable Power Generation Costs in 2018. Available online: https://www.irena.org/-/media/Files/IRENA/Agency/Publication/2019/May/IRENA_Renewable-Power-Generations-Costs-in-2018.pdf (accessed on 18 September 2024).
31. Annual Energy Outlook 2018 with Projections to 2050. Available online: https://downloads.regulations.gov/EPA-HQ-OAR-2017-0357-0060/attachment_45.pdf (accessed on 18 September 2024).
32. Global Trends in Renewable Energy Investment 2019. Available online: https://www.fs-unep-centre.org/wp-content/uploads/2019/11/GTR_2019.pdf (accessed on 18 September 2024).
33. Röger, M.; Lüpfert, E.; Caron, S.; Dieckmann, S. Techno-economic analysis of receiver replacement scenarios in a parabolic trough field. *AIP Conf. Proc.* **2016**, *1734*, 030030.
34. Study of Equipment Prices in the Power Sector. Available online: https://documents1.worldbank.org/curated/en/952421468330897396/pdf/817250ESM0ESMA0Box0379844B00PUBLIC0.pdf (accessed on 18 September 2024).
35. Staffell, I.; Green, R. How does wind farm performance decline with age? *Renew. Energy* **2014**, *66*, 775–786. [CrossRef]
36. Padilla, R.V. Simplified Methodology for Designing Parabolic Trough Solar Power Plants. Ph.D Thesis, University of South Florida, Tampa, FL, USA, 4 April 2011.
37. Haas, J.; Cebulla, F.; Nowak, W.; Rahmann, C.; Palma-Behnke, R. A multi-service approach for planning the optimal mix of energy storage technologies in a fully-renewable power supply. *Energy Convers. Manag.* **2018**, *178*, 355–368. [CrossRef]
38. Han, X.; Lu, L.; Zheng, Y.; Feng, X.; Li, Z.; Li, J.; Ouyang, M. A review on the key issues of the lithium ion battery degradation among the whole life cycle. *eTransportation* **2019**, *1*, 100005. [CrossRef]
39. Wetter, M.; Wright, J. Comparison of a Generalized Pattern Search and a Genetic Algorithm Optimization Method. In Proceedings of the Eighth International IBPSA Conference, Eindhoven, The Netherlands, 11–14 August 2003.
40. Hanrieder, N.; Sengupta, M.; Xie, Y.; Wilbert, S.; Pitz-Paal, R. Modeling beam attenuation in solar tower plants using common DNI measurements. *Sol. Energy* **2016**, *129*, 244–255. [CrossRef]
41. Perdichizzi, A.; Barigozzi, G.; Franchini, G.; Ravelli, S. Peak shaving strategy through a solar combined cooling and power system in remote hot climate areas. *Appl. Energy* **2015**, *143*, 154–163. [CrossRef]